

Dynamic compression properties of E-glass/basalt and E-glass/flax using SHPB

Muhamad Shahirul Mat Jusoh^{1,*}, Mohd Yazid Yahya², Haris Ahmad Israr Ahmad²

¹⁾ Department of Polymer Composite Processing Engineering Technology, Kolej Kemahiran Tinggi MARA Masjid Tanah, Persiaran Paya Lebar, Ramuan China Besar, 78300 Masjid Tanah, Melaka, Malaysia

²⁾ School of Mechanical Engineering, Universiti Teknologi Malaysia, 81310, Skudai, Johor, Malaysia

*Corresponding e-mail: shahirul.jusoh@mara.gov.my

Keywords: SHPB; hybrid; composite

ABSTRACT – Investigation on the dynamic compression properties of natural fibres hybrid composites is less reported especially using split Hopkinson pressure bar (SHPB) due to the availability of dynamic testing apparatus. The split Hopkinson pressure bar (SHPB) was utilized in this present study to characterize the dynamic mechanical properties of hybrid composite between E-glass with basalt and flax fibres at the strain rates of 850 to 2350 s⁻¹. Result shows that the tested specimens significantly influenced by the value of strain rates applied. The hybrid composites of E-glass/basalt (E/B_{basalt}) and E-glass/flax (E/F_{flax}) exhibited the strain-rate dependent, whereby the higher of dynamic compression properties were recorded when the higher strain rates were imposed. Both hybrid specimens exhibited the similar trend.

1. INTRODUCTION

The strain-rate effect is widely recognised as a crucial factor influencing the mechanical properties of material [1]. The hybrid composite of hemp/glass was characterized using SHPB with its dynamic compression properties was recorded between the glass and hemp laminates [4]. Natural fibres of pultruded jute and kenaf reinforced composites were investigated experimentally using SHPB at different strain rates of 1021, 1150, and 1340 s⁻¹. The higher of dynamic compression properties were recorded when the tested specimen was imposed at 1340 s⁻¹ rather than 1021 s⁻¹ [2]. Previous study revealed that the strain rate effects of the composite materials are highly correlated with materials hardening factors as tested on the hybrid composite of carbon/glass. Three different strain rates of 200, 600, and 1000 s⁻¹ were imposed and found significantly influenced on the properties of the material being investigated. In addition, there are few contributed factors involved such as types of materials used, manufacturing process, surficial adhesion between fibre and matrix, fibre architecture and loading direction [3]. The SHPB test was applied on the rice husk/linear low-density PE with the strain rates of 650, 900, and 1100 s⁻¹. The higher of dynamic compression strength and modulus were recorded with the increasing strain rates [5]. The objectives of the present work are to investigate the influence of the different high strain rates on the stress-strain curves of E/B_{basalt} and E/F_{flax} using SHPB.

2. METHODOLOGY

The hybrid composites of E/B_{basalt} and E/F_{flax} were fabricated using vacuum infusion process. Dynamic compression test was conducted using SHPB at the strain rates between 850 to 2350 s⁻¹. Figure 1 shows the schematic diagram of SHPB equipment which consists of gun barrel, striker bar, incident bar and transmitter bar. All the bars should maintain their elasticity throughout the test.

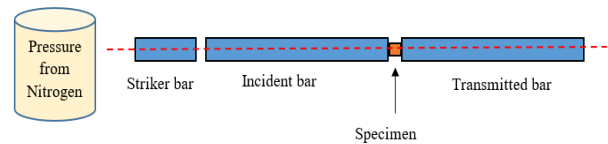
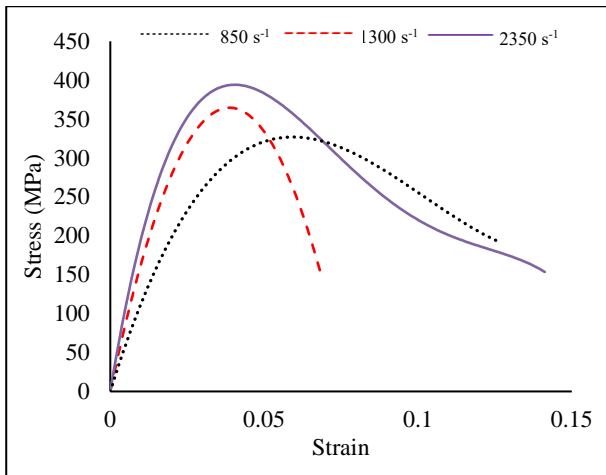
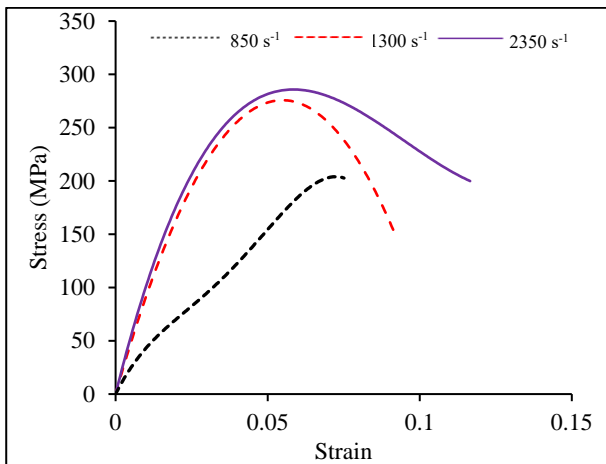


Figure 1 SHPB setup.

During the test, generated pressure from nitrogen tank will accelerate the striker bar, then collide with the incident bar. As a result of collision, the compression wave was generated and travelled down along the incident bar and known as incident wave (ϵ_i). Meanwhile, at the specimen interface, the wave was partially transmitted into the specimen and referred as transmitted wave (ϵ_t). The remaining wave was reflected and known as reflected wave (ϵ_r) due to the impedance mismatch between the incident bar and the specimen.

3. RESULTS AND DISCUSSION

As shown in Figure 2 and 3, the stress-strain curves of E/B_{basalt} and E/F_{flax} composites had been dominated by the strain rates effect. The higher the strain rates imposed, the higher the maximum stress exhibited by the tested specimens. The E/B_{basalt} and E/F_{flax} composites recorded the maximum compressive stress of 387, 328, 300 and 283, 247, 214 MPa at the strain rates of 2350, 1300, and 850 s⁻¹, respectively. Similar findings were also reported by the previous literatures [2], [5]–[8] and the increment is attributed by the strengthening effect of the material towards the strain rate applied as suggested by Omar et al. [7]. Conversely, the dynamic failure strain decreases with the increasing strain rates for both tested hybrid composites due the rapid crack propagation and fibre's failure occurred within a very short time which caused the total failure of the specimens, as stipulated in previous literatures [1].

Figure 2 Stress-strain curves of E/B_{asalt}.Figure 3 Stress-strain curves of E/F_{Iax}.

4. CONCLUSION

This study explored the high strain rates effect on the dynamic compression properties of E/B_{asalt} and E/F_{Iax} at the strain rates of 850, 1300, and 2350 s⁻¹. It was found that the dynamic properties were dependent on the applied strain rates with the E/B_{asalt} dominated on the maximum compressive stress compared to E/F_{Iax}. However, the dynamic strain recorded the contrary pattern with increasing strain-rates with E/F_{Iax} recorded the lower strain than E/B_{asalt}. It can be concluded that the effect of hybridisation significantly affected on the dynamic compression properties as revealed between E/B_{asalt} and E/F_{Iax}.

ACKNOWLEDGEMENT

Authors would like to thank to Kolej Kemahiran Tinggi MARA (KKTMM) Masjid Tanah, Melaka for providing research fund to support this study and has made this work possible.

REFERENCES

- [1] Song, Z., Wang, Z., Ma, H., & Xuan, H. (2014). Mechanical behavior and failure mode of woven carbon/epoxy laminate composites under dynamic compressive loading. *Composites Part B: Engineering*, 60, 531-536.
- [2] Omar, M. F., Akil, H. M., Ahmad, Z. A., Mazuki, A. A. M., & Yokoyama, T. (2010). Dynamic properties of pultruded natural fibre reinforced composites using split Hopkinson pressure bar technique. *Materials & Design*, 31(9), 4209-4218.
- [3] Zhu, P., Lu, J., Ji, Q., & Cheng, Z. (2016). Experimental study of in-plane mechanical performance of carbon/glass hybrid woven composite at different strain rates. *International Journal of Crashworthiness*, 21(6), 542-554.
- [4] Kim, W., Argento, A., Lee, E., Flanigan, C., Houston, D., Harris, A., & Mielewski, D. F. (2012). High strain-rate behavior of natural fiber-reinforced polymer composites. *Journal of Composite Materials*, 46(9), 1051-1065.
- [5] Wahab, A., Suhaili, N., Omar, M. F., Md Akil, H., Ahmad, Z. A., & Noimam, N. Z. (2016). Effect of surface modification on rice husk (Rh)/linear low density polyethylene (LLDPE) composites under various loading rates. *Materials Science Forum*, 840, 3-7.
- [6] Akil, H. M., Ahmad, Z. A., Omar, M. F., Lin, O. H., & Hui, D. (2010). Measurement on the dynamic properties of nanosilica/polypropylene composite using split Hopkinson pressure bar technique, *University of New Orleans*. 1-3.
- [7] Omar, M. F., Akil, H. M., & Ahmad, Z. A. (2011). Measurement and prediction of compressive properties of polymers at high strain rate loading. *Materials & Design*, 32(8-9), 4207-4215.
- [8] Suharty, N. S., Ismail, H., Diharjo, K., Handayani, D. S., & Firdaus, M. (2016). Effect of kenaf fiber as a reinforcement on the tensile, flexural strength and impact toughness properties of recycled polypropylene/halloysite composites. *Procedia Chemistry*, 19, 253-258.

Multiple linear regression application for generating entropy characteristics of magnesium alloy

M.A. Fauthan^{1,*}, S. Abdullah¹, M.F. Abdullah², I.F. Mohamed¹

¹) Centre for Integrated Design for Advanced Mechanical Systems (PRISMA), Faculty of Engineering & Built Environment, Universiti Kebangsaan Malaysia, 43600 UKM Bangi, Selangor, Malaysia

²) Department of Mechanical Engineering, Faculty of Engineering, Universiti Pertahanan Nasional Malaysia, Kem Sg. Besi 57000 Kuala Lumpur, Malaysia

*Corresponding e-mail: p85968@siswa.ukm.edu.my

Keywords: Magnesium alloy; entropy; multiple linear regression

ABSTRACT – This paper focused on the development of a multiple linear regression approach based on the stress ratio and applied load. This relationship was developed for the purpose of predicting a complete entropy generation by means of a statistical approach, whereby a constant amplitude loading was applied to evaluate the fatigue life. By conducting compact tension tests, different stress ratios of 0.1, 0.4 and 0.7 were applied to the specimen. During the tests, the change in temperature was also observed. The assumptions of the models were considered through a graphical residual analysis. As a result, the predicted regression model based on the applied load and stress ratio was found to be in agreement with the results of the experiment.

1. INTRODUCTION

The selection of magnesium alloy for applications in, for example, the aerospace, automotive and electronic industries, is becoming more important as this material offers admirable features such as high stiffness, light weight, high specific strength, and good heat conductivity. Since magnesium alloy is a relatively new material compared to mild structural steel and aluminium, further investigations are needed to ensure its safe application. A major problem with structural systems is fatigue failure since there is no significant indication that failure is about to occur. This is because failure can occur even with a low load if it is applied repeatedly. Therefore, crack propagation plays a key role in determining the life span of a component.

Fatigue is probabilistic in nature and involves, at the same time, a multimode process. In a conventional test, many unknown input parameters are required. Therefore, the dissipation of energy is introduced to predict the life span of a material [1]. Furthermore, this relationship can also be described through the introduction of multiple linear regression (MLR). MLR is used to predict the value of a variable based on the values of two or more other variables [2]. Mayan et al. suggested multiple linear regression in order to evaluate the number of cycles, stress amplitude and crack length of aluminium alloy [3]. If the total generation of entropy can be approached through regression, then fatigue life can be predicted. Hence, this paper was aimed at describing the MLR relationship in order to predict the total entropy generation of magnesium alloy, AZ31B.

2. MATERIAL AND EXPERIMENTAL PROCEDURE

This study utilised the commercial AZ31B magnesium alloy. The mechanical properties of the AZ31B is listed in Table 1.

Table 1 Mechanical properties of AZ31B [1].

Properties	Yield strength, σ_s (MPa)	Ultimate strength, σ_{UTS} (MPa)	Young's modulus, E (GPa)
AZ31B	144	238	40.66

To study the fatigue crack growth (FCG), compact tension (CT) test specimens were prepared according to the recommendations of E647-95. Before the fatigue tests, the surface of the specimens facing the thermal sensor was coated with a layer of black paint to improve the thermal emissivity and to reduce the error rate.

All the specimens were tested using a constant amplitude sinusoidal loading of 2600 N and 2800 N, and stress ratios (ratio of minimum to maximum load) of $R = 0.1, 0.4$ and 0.7 , respectively at a constant frequency of 10 Hz. During the test, the temperature trend of the specimens was detected with an infrared sensor that had been set up.

The total entropy generation was obtained from the beginning of the FCG test until the occurrence of fracture, and it was calculated as shown below:

$$\dot{\gamma} = \frac{W_p}{T} \quad (1)$$

Where $\dot{\gamma}$ is the entropy generation rate, W_p is cyclic plastic energy per unit volume and T is surface temperature.

Multiple regression analysis is statistical method used for predicting the unknown value of a variable from the known value of two or more variable [2]. The general multiple regression model with n observations is defined as:

$$y_1 = \alpha + \beta_1 x_{i,1} + \beta_2 x_{i,2} + \dots + \beta_n x_{i,n} + \varepsilon_i \quad (2)$$

Where y is a variable, x is the independent variable, and β is the unknown regression coefficient.

3. RESULTS AND DISCUSSION

For the load of 2600 N, just after the cycles reached 4.34×10^3 for a stress ratio of 0.1, the crack began to grow, followed by 3.73×10^3 and 2.28×10^3 cycles for stress ratios of 0.4 and 0.7, respectively. As shown in Figure 1, the final crack cycle was lower when a higher stress ratio was applied. This also affected the fatigue crack growth rate, causing it to increase as the mean stress value changed. This trend was followed by the load of 2800 N, when stress ratios of 0.1, 0.4 and 0.7 were applied to the specimen.

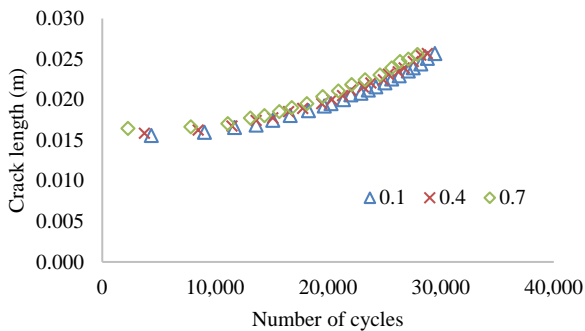


Figure 1 Crack length reading for 2600N at stress ratio of 0.1, 0.4 and 0.7.

At the start of the test, no entropy was generated. As the crack growth increased, the total entropy was calculated until the specimen fractured completely. The total entropy generation when a load of 2600 N was applied was 3.424, 3.101 and 2.922 $\text{MJm}^{-3} \text{K}^{-1}$ for stress ratios of 0.1, 0.4 and 0.7, respectively. According to Figure 2, the total entropy generation increased as a higher stress ratio was applied. This was due to the distribution of a higher energy per unit volume, which led to failure. It showed that with a higher entropy generation, the specimen should have a lower fatigue life.

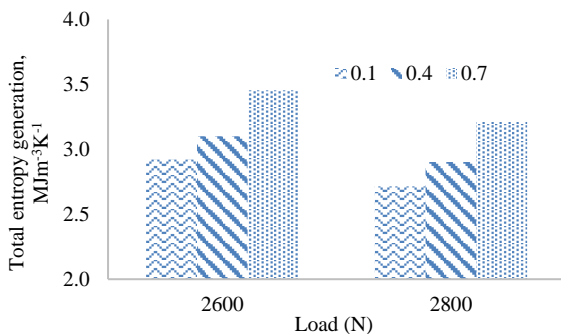


Figure 2 Total entropy generation with different loads and stress ratios.

Next, the assumptions of the MLR model were assessed. The four different conditions that need to be evaluated for multiple regression to give a valid result are the linear function, independent function, normal distribution and equal variance. The results are shown in Figure 3. The versus fits plot shows that the average of the residuals remained approximately 0, the variation of the residuals appeared to be roughly constant, and there were no excessively outlying points. There was little in the histogram of the residuals to suggest a violation of the normality assumption.

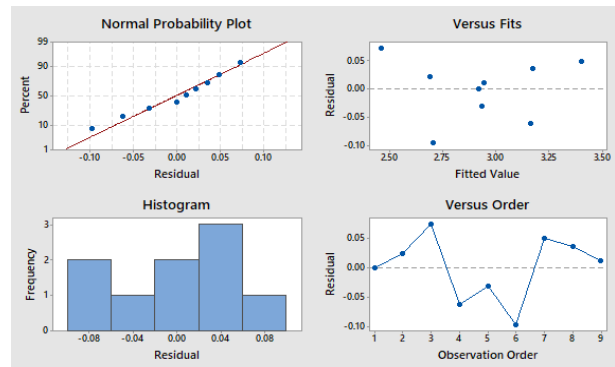


Figure 3 Observation of multiple regression to evaluate data from experiment for MLR model.

The datasets comprising the entropy generation values of the CT specimens, stress ratio (R), and load applied (N), as shown in Eqn. 3, were used to establish the MLR-based entropy models. The MLR-based entropy generation model was obtained as:

$$\gamma = 5.827 - 0.001148 N + 0.8044R \quad (3)$$

Table 2 The percentage of difference entropy generation with respect to the experimental data.

Stress ratio	Experimental entropy	Predicted entropy	% of differences
0.1	2.536	2.608	2.83%
0.4	2.607	2.849	9.29%
0.7	2.956	3.090	4.55%

Once the assumption on MLR-based entropy model had been clarified to be acceptable, the models were compared to the experimental values done with another new load, 3000 N. Table 2 shows the percent of difference between the experimental and predicted data for new load conditions. The difference is less than 10%, and this indicates that the calculated entropy generation well predicts the experimental data under new load conditions. This explains most of the experimental entropy generation were near to similar predicted values.

4. CONCLUSION

Entropy generation was deployed as an effective way of measuring the crack growth behaviour of a material with changes in the temperature during the fatigue process. An approach to develop an MLR relationship between the entropy generation, applied load, and stress ratio was shown in this paper. The results were indeed encouraging, where the percentage difference between the MLR-based entropy models was less than 10%, indicating that the entropy values obtained from the experiment and regression model were in good agreement.

ACKNOWLEDGEMENT

The authors graciously acknowledge the financial support provided by Universiti Kebangsaan Malaysia.

REFERENCES

- [1] Xu, Z., Zhang, H., Yan, Z., Liu, F., Liaw, P. K., & Wang, W. (2017). Three-point-bending fatigue behavior of AZ31B magnesium alloy based on

- infrared thermography technology. *International Journal of Fatigue*, 95, 156-167.
- [2] Kong, Y. S., Abdullah, S., Schramm, D., Omar, M. Z., & Haris, S. M. (2019). Development of multiple linear regression-based models for fatigue life evaluation of automotive coil springs. *Mechanical Systems and Signal Processing*, 118, 675-695.
- [3] Mayén, J., Abúndez, A., Pereyra, I., Colín, J., Blanco, A., & Serna, S. (2017). Comparative analysis of the fatigue short crack growth on Al 6061-T6 alloy by the exponential crack growth equation and a proposed empirical model. *Engineering Fracture Mechanics*, 177, 203-217.

Microhardness and sound velocity characterization of heat treated AISI 1050 carbon steel

Zakiah Abd Halim^{1,2,*}, Nur Farah Hani Nor Alzahari^{1,2}

¹⁾ Fakulti Kejuruteraan Mekanikal, Universiti Teknikal Malaysia Melaka, Hang Tuah Jaya, 76100 Durian Tunggal, Melaka, Malaysia

²⁾ Centre for Advanced Research on Energy, Universiti Teknikal Malaysia Melaka, Hang Tuah Jaya, 76100 Durian Tunggal, Melaka, Malaysia

*Corresponding e-mail: zakiahh@utem.edu.my

Keywords: Microhardness; sound velocity; heat treatment

ABSTRACT – This paper investigates the microhardness and sound velocity of heat treated AISI 1050 carbon steel. Three samples were subjected to different austenization temperatures of 800°C, 900°C and 1000°C for 30 minutes and then water-quenched, followed by tempering at 300°C for 50 minutes. Microhardness testing and ultrasonic testing were performed on the specimen before and after each heat treatment processes. It was observed that the hardness of the AISI 1050 carbon steel has inversed relationship with the sound velocity. The results show the sound velocity are affected by the type of heat treatment process.

1. INTRODUCTION

Heat treatment process is a process of heating and cooling a metal that is widely used to modify the mechanical properties of materials such as hardness, machinability and formability [1]. Medium carbon steel such as AISI 1050 is widely used for high quality cutting components, surgery equipment and small ball bearing due to its renowned properties of high hardness and subsequently high wear resistance. The high hardness is achieved through heat treatment processes such as quenching and tempering to suit the specific applications. Up to date, the research on mechanical properties on heat treated metal mainly focus on the influence of microstructure properties [2]. These methods are destructive and impair the usability of the future usefulness of the material. Literatures on non-destructive characterization of the mechanical properties is very scant. Previous studies successfully used ultrasonic testing to characterize the hardness and microstructures of heat treated and welded joints [3,4]. The request for fast and reliable non-destructive characterization of material properties after heat treatment is increasing due to its advantages over destructive testing. This paper studies the effect of quenching and tempering on the sound velocity and microhardness of AISI 1050 medium carbon steel. Characterization of material properties non-destructively enable cutting down testing time and ensure that the material can be reused after the test.

2. METHODOLOGY

The material in this study was carbon steel AISI 1050. The material composition consists of carbon (0.47-0.55%), sulphur ($\leq 0.05\%$), manganese (0.60-0.90%), phosphorus ($\leq 0.47\%$) and iron (98.4–98.92%). The material has dimension of 20 mm × 20 mm × 10 mm.

There were four specimens involved in this study. The sample designation and its heat treatment conditions are tabulated in Table 1. One specimen was used as a control specimen and three specimens were subjected to different austenization temperatures, which are 800°C, 900°C and 1000°C.

Table 1 Details of heat treatment conditions.

Sample	Austenization temperature	Quenching medium	Tempering temperature
R	-	-	-
A	800	Water	300
B	900	Water	300
C	1000	Water	300

The time taken for heating the specimen in the furnace from room temperature was set to 15 minutes and then was hold at the austenization temperature for 30 minutes. The specimens were then quenched into water. The specimens were then reheated and held at tempering temperature for 50 minutes. The specimen were air cooled to room temperature. The heat treatment processes for the specimen were summarized in Figure 1.

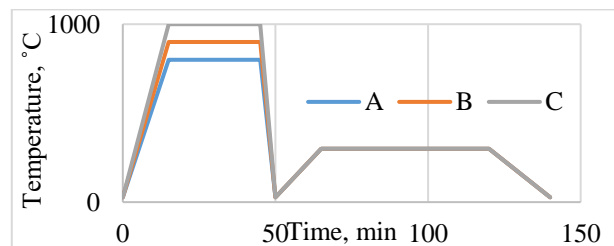


Figure 1 Temperature profile of heat treatment process on AISI 1050.

Ultrasonic tester USM35 and 5MHz ultrasonic sensor as illustrated in Figure 2 were used to measure the sound velocity of the specimen at all stages of the heat treatment process. The sensor was calibrated using International Institute of Welding reference block. Oil couplant was used to facilitate the longitudinal ultrasonic transmission from the sensor and reflection from the material. The sound velocity of heat treated, V_h was determined by thickness scaling factor between calibrated specimen thickness, t_c and measured thickness, t_h with the sound velocity of calibrated specimen, V_c using Equation (1).

$$V_h \text{ (m/s)} = \frac{\text{Calibrated thickness, } t_c \text{ (mm)}}{\text{Measured thickness, } t_h \text{ (mm)}} \times V_c \text{ (m/s)} \quad (1)$$

The hardness of the specimen was verified by Vickers microhardness testing. The average of ten indentations were taken for each specimen to represent the hardness of the materials before and after subjected to quenching as well as tempering.

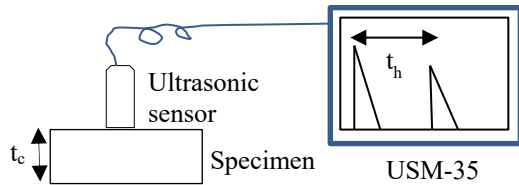


Figure 2 Sound velocity measurement.

3. RESULTS AND DISCUSSION

Figure 3 depicts the effect of quenching temperature on AISI 1050 medium carbon steel. It was observed that the hardness of AISI 1050 increased to slightly more than 400 HV when subjected to quenching compared to its initial hardness of 200 HV. However, the sound velocity of AISI 1050 did not show significant differences from its initial of 5960 m/s when subjected to different quenching temperature.

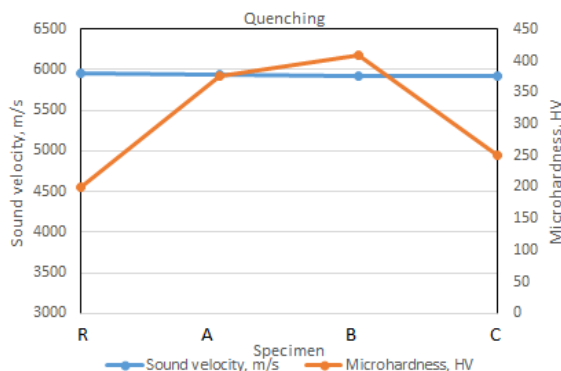


Figure 3 Sound velocity and microhardness of AISI 1050 after quenched.

Figure 4 portrays that the tempering process reduced the high hardness of AISI 1050 to 250 HV. There was a significant difference shown by the tempered specimens. The high hardness shown by quenched materials were reduced by tempering the materials. It was observed that the sound velocity in the AISI 1050 also decreased significantly to 4000 m/s from the initial sound velocity. The result obtained indicates that the sound emission in the heat treated specimen are affected by the type of heat treatment process. Quenching produced martensite microstructure that contains high stress [5]. Hence it is difficult for sound to propagate in the specimen. Tempering relieves the stress inside the specimen and form a more stable microstructure of pearlite [6]. At similar specimen thickness, the time taken for the sound to be reflected in quenched specimen was longer compared after it was tempered. The hardness of sample C reduced to 250 HV as transformation above 950°C retained austenite, which reflected low hardness for both heat treatment [2].

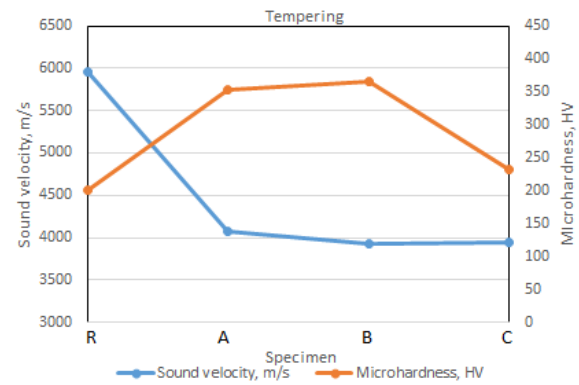


Figure 4 Sound velocity and microhardness of AISI 1050 after quenched and tempered.

4. CONCLUSION

A non-destructive material characterization of heat treated AISI 1050 using sound velocity has been proposed in this paper. Both quenching and tempering processes increased the hardness of material. It was found that quenching temperature does not affect the sound velocity of the material, but the tempering process shown a significant change in sound velocity. The sound velocity is dependent on the type of heat treatment. Verification of microstructural is needed to form a strong relationship for non-destructive evaluation of material properties.

ACKNOWLEDGEMENT

The authors gratefully acknowledged the financial support from Universiti Teknikal Malaysia Melaka (UTeM) under Short Term Grant Scheme with reference no. PJP/2019/FKM(8B)/S01680.

REFERENCES

- [1] Bryson, W. E. (2005). *Heat treatment, selection, and application of tool steels*. Hanser Gardner Publications.
- [2] Essoussi, H., Elmouhri, S., Ettaqi, S., & Essadiqi, E. (2019). Heat treatment effect on mechanical properties of AISI 304 austenitic stainless steel. *Procedia Manufacturing*, 32, 883-888.
- [3] Uzun, F., & Bilge, A. N. (2015). Application of ultrasonic waves in measurement of hardness of welded carbon steels. *Defence Technology*, 11(3), 255-261.
- [4] Ruiz, A., Fuentes-Corona, K. J., López, V. H., & León, C. A. (2017). Microstructural and ultrasonic characterization of 2101 lean duplex stainless steel welded joint. *Applied Acoustics*, 117, 12-19.
- [5] de Araújo Freitas, V. L., de Albuquerque, V. H. C., de Macedo Silva, E., Silva, A. A., & Tavares, J. M. R. (2010). Nondestructive characterization of microstructures and determination of elastic properties in plain carbon steel using ultrasonic measurements. *Materials Science and Engineering: A*, 527(16-17), 4431-4437.
- [6] El Rayes, M. M., El-Danaf, E. A., & Almajid, A. A. (2015). Ultrasonic characterization of heat-treatment effects on SAE-1040 and-4340 steels. *Journal of Materials Processing Technology*, 216, 188-198.

Investigation on the effects of electrospinning distance and applied voltage on morphology of poly(vinyl alcohol) electrospun nanofibres

Abdul Hamid Nurfaizey^{1,2,*}, Fatin Hanani Abdullah¹, Siti Hajar Sheikh Md Fadzullah^{1,2}, Zaleha Mustafa³, Mohd Azli Salim^{1,2}, Mohd Zaid Akop^{1,2}

¹⁾ Fakulti Kejuruteraan Mekanikal, Universiti Teknikal Malaysia Melaka, Hang Tuah Jaya, 76100 Durian Tunggal, Melaka, Malaysia

²⁾ Centre for Advanced Research on Energy, Universiti Teknikal Malaysia Melaka, Hang Tuah Jaya, 76100 Durian Tunggal, Melaka, Malaysia

³⁾ Fakulti Kejuruteraan Pembuatan, Universiti Teknikal Malaysia Melaka, Hang Tuah Jaya, 76100 Durian Tunggal, Melaka, Malaysia

*Corresponding e-mail: nurfaizey@utem.edu.my

Keywords: Electrospinning; electrospun nanofibre; electrospinning distance; fibre diameter

ABSTRACT- In electrospinning process, the applied voltage and electrospinning distance are the two most important parameters that affect the quality of the fibres. In this study, these two parameters were studied. Polyvinyl alcohol (PVOH) electrospun fibres were produced using electrospinning technique. The morphology and fibre diameter of the fibres were examined using scanning electron microscopy and ImageJ. From the results, fibre diameter decreased when electrospinning distance decreased. However, there was no direct relationship between applied voltage and fibre diameter. The best electrospinning parameters were 10 kV of applied voltage and 10 cm of electrospinning distance.

1. INTRODUCTION

Electrospinning process is a version of electrospraying process which involves high electric potentials to charge a liquid, forcing the liquid to disperse onto an oppositely charged or grounded collector electrode [1]. The main difference is that in electrospinning, the liquid does not break up into fine droplets but instead forming strands of ultra-fine fibres when collected at the collector electrode.

There are several crucial parameters that influence the morphology of electrospun fibres such as flow rate, solution concentration, distance between the nozzle and the collector and the applied voltage. This study investigates the effect of the different applied voltage and the distance from the nozzle to the collector on the morphology of electrospun polyvinyl alcohol nanofibres. The best parameters for producing thin and defect free nanofibres were also determined.

2. METHODOLOGY

Poly(vinyl alcohol) or PVOH pellets with an average molecular weight of 124,000-130,000 g/mol and distilled water were mixed to get 8 wt.% of final concentration. The solution was stirred using IKA RW20 digital stirrer machine for 6 hours until a clear solution was obtained. A laboratory scale electrospinning machine, Electrospin Model ES1a (Electrospin Ltd., NZ) was used throughout the study. The flow rate was set at 1.100 ml/h. Samples were collected at various combinations of applied voltages

and electrospinning distances. The samples were sputtered with platinum in JEOL JEC-300FC auto fine coated machine for 180 seconds. The samples were scanned under scanning electron machine Model JSM-6010PLUS/LV (JEOL Ltd., Japan) to observe the morphology of electrospun nanofibres. The average fibre diameter of nanofibres was measured based on SEM micrographs using IMAGEJ software.

3. RESULTS AND DISCUSSION

Figure 1 and 2 show the SEM micrographs of the samples. For the first experiment, fibres started to produce at 10 kV of applied voltage. From the Figure 1 (a) and (b), solid and smooth fibres were produced when the applied voltage was at 10 kV to 15 kV. However, increasing the applied voltage further to 35 kV, abnormal fibres started to form that randomly interconnected to each other (Figure 1(f)). This was because at 35 kV, the fibres were being withdrawn at a very high speed due to excessive applied electric forces. In the second experiment, a wet film of polymer was formed at short distance of 2.5 cm (Figure 2 (a)). This happened because the solvent did not have enough time to evaporate before reaching the collector. The production rate of the fibres was also decreased as the electrospinning distance increased as evidenced in Figure 2 (b) to Figure 2 (g).

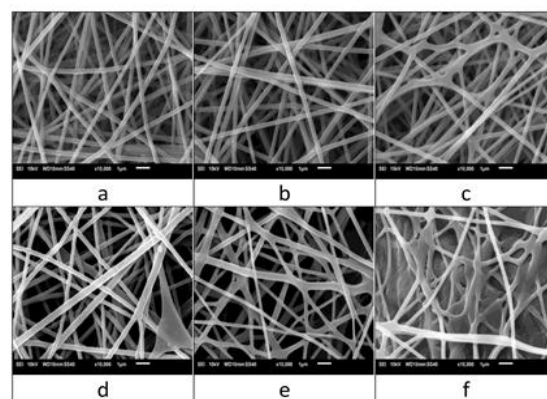


Figure 1 SEM micrographs of samples ($\times 10,000$ magnification) produced at different applied voltages of (a) 10kV (b) 15kV (c) 20kV (d) 25kV (e) 30kV (f) 35kV.

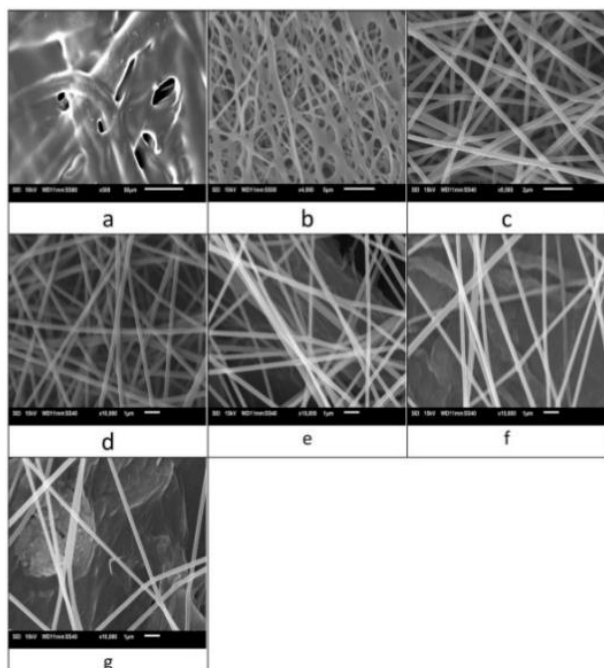


Figure 2 SEM micrographs of samples ($\times 10,000$ magnification) produced at different electrospinning distances of (a) 2.5cm (b) 5cm (c) 7.5cm (d) 10cm (e) 12.5cm (f) 15cm (g) 17.5 cm.

The average fibre diameters of all samples are presented in Figure 3 and Figure 4. From Figure 3, the diameter of the fibres decreased as the distance increased. A similar finding was reported by Jayesh Doshi et al. [2]. This happened because extending the distance also prolonged the fibre's stretching time, thus producing finer fibres [3-4].

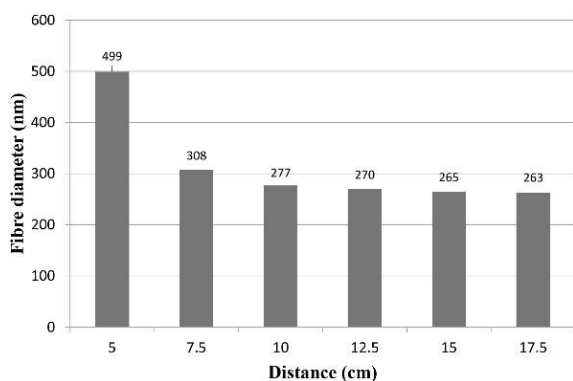


Figure 3 Fibre diameter as a function of electrospinning distance.

From Figure 4, there was no significant relationship between fibre diameter and applied voltage. Although a high applied voltage is required to form smooth fibres, however excessive applied electric forces could also cause the fibres to be prematurely deposited onto the collector as shown previously in Figure 1(f).

From the experiment, the best electrospinning parameters were 10 kV of applied voltage and 10 cm of electrospinning distance. At these parameters, the diameter of the fibres was consistent at 277 ± 25 nm.

Furthermore, there were no sign of abnormal fibres such as beaded fibres or flat fibres.

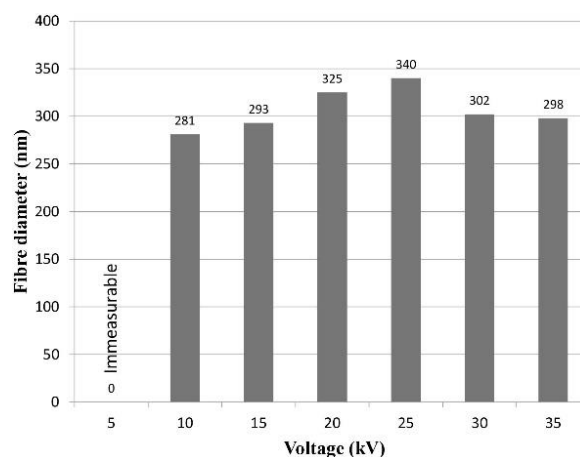


Figure 4 Fibre diameter as a function of applied voltage.

4. CONCLUSION

In this study, the effects of applied voltage and electrospinning distance on the morphology of PVOH electrospun fibres were studied. Extending the electrospinning distance would decrease the fibre diameter, however increasing the applied voltage would not directly relate to fibre diameter. The best electrospinning parameters were 10 kV of applied voltage and 10 cm of electrospinning distance.

ACKNOWLEDGEMENT

This work is funded by FRGS/2018/FKM-CARE/F00372 Ministry of Education Malaysia. Special thanks to Fakulti Kejuruteraan Mekanikal, Universiti Teknikal Malaysia Melaka (UTeM).

REFERENCES

- [1] Pillay, V., Dott, C., Choonara, Y. E., Tyagi, C., Tomar, L., Kumar, P., ... & Ndesendo, V. M. (2013). A review of the effect of processing variables on the fabrication of electrospun nanofibers for drug delivery applications. *Journal of Nanomaterials*, 2013.
- [2] Doshi, J., & Reneker, D. H. (1995). Electrospinning process and applications of electrospun fibers. *Journal of electrostatics*, 35(2-3), 151-160.
- [3] Doustgani, A. (2015). Effect of electrospinning process parameters of polycaprolactone and nanohydroxyapatite nanocomposite nanofibers. *Textile Research Journal*, 85(14), 1445-1454.
- [4] Long, F., Kamsom, R., Nurfaizey, A., Isa, M., & Masripan, N. (2017). The influence of electrospinning distances on fibre diameter of poly (vinyl alcohol) electrospun nanofibers. *Proceedings of Mechanical Engineering Research Day 2017*, 377-378.

A study on tensile properties of poly(vinyl alcohol) electrospun nanofibers

Abdul Hamid Nurfaizey^{1,2,*}, Nor Amalina Azmi¹, Nor Azmmi Masripan^{1,2}, Zaleha Mustafa³, Adzni Md. Saad^{1,2}, Faizil Wasbari^{1,2}

¹) Fakulti Kejuruteraan Mekanikal, Universiti Teknikal Malaysia Melaka, Hang Tuah Jaya, 76100 Durian Tunggal, Melaka, Malaysia

²) Centre for Advanced Research on Energy, Universiti Teknikal Malaysia Melaka, Hang Tuah Jaya, 76100 Durian Tunggal, Melaka, Malaysia

³) Fakulti Kejuruteraan Pembuatan, Universiti Teknikal Malaysia Melaka, Hang Tuah Jaya, 76100 Durian Tunggal, Melaka, Malaysia

*Corresponding email: nurfaizey@utem.edu.my

Keywords: Electrospinning; nanofibres; tensile test

ABSTRACT - Electrospinning is an easy and flexible method for the production of nanofibers. It has generated a great amount of interest for use in many areas, mainly due to its high surface area. For these applications, it is important to understand the mechanical properties of this material. In this study, tensile strength of polyvinyl alcohol (PVOH) electrospun fibres was investigated. PVOH nanofibres were produced using electrospinning method. The morphology of the fibres was observed under scanning electron microscopy (SEM). The tensile properties of PVOH were examined according to ASTM D882: *Standard Test Method for Tensile Properties of Thin Plastic Sheeting* using a universal tensile machine. The average tensile strength was found to be 2.5838 MPa which was comparable to previous studies.

1. INTRODUCTION

Nanofibers are defined as fibres with diameters below 100 nm [1]. To date, nanofibres have been produced from a wide range of materials, including natural polymers, synthetic polymers, carbon based nanomaterials, semi-conducting nanomaterials and composite nano-materials [2]. Currently, there are three techniques available for the synthesis of nanofibers: electrospinning, self-assembly, and phase separation. Of these techniques, electrospinning is the most widely studied technique due to its simple configuration, the ability to mass produce continuous nanofibres from different polymers and the ability to mass produce continuous nanofibres from different polymers [3]. Because of their high volume surface area, high porosity and interconnected permeable network [2], electrospun nanofibers have been proposed for a wide variety of applications such as filtration, tissue engineering scaffolds, drug delivery system and sensor [4]. In electrospinning, focus is normally given on the production of uniform fibres and how the diameter values and their distribution can vary with the materials and the processing conditions [5]. However, there is little information about the structure of nanofibers, the

mechanical properties that accompany them and how they vary with the processing conditions. Therefore, it is important to understand the nature of the process and the tensile properties of the fibres. In this study, tensile strength of poly(vinyl alcohol) (PVOH) electrospun fibres was investigated.

2. MATERIALS AND METHODS

PVOH with an average molecular weight of 124,000-130,000 g/mol and degree of hydrolysis (DH) of 86-89% was obtained from Polyscientific, Malaysia. The polymer solution was prepared by weighing the PVOH pellets and distilled water using a digital weighing balance machine to a final concentration of 8 wt.%. It was then placed on an IKA RW20 digital stirrer for 6 hours using a stirring speed of 380 rpm. The solutions were electrospun immediately after preparation. The setup used for electrospinning Electrospinz Model ES1a (Electrospinz Ltd., NZ) with 1.100 ml/h of flow rate. The electrospinning process was carried out for a period of 60 minutes. The distance from the tip of the needle to the collector was 10 cm and the applied voltage was 20 kV. The collected samples were sputtered with platinum using JEOL JEC-300FC auto fine coating machine for 180 seconds. The average fibre diameter was measured using ImageJ software based on SEM micrograph obtained earlier. Tensile test was conducted according to ASTM D882 using a universal testing machine (200 Series Single Column Test Machines, Shimadzu) with a load cell of 1 kN. Five dumbbells shaped specimens were cut using Super Dumbbell Cutter (SD lever controlled, Model SDL-100). The average thickness of the film for the electrospun samples was 0.01mm, which was measured using a digital micrometre (Mitutoyo, 293-340). The size of the specimens were approximately 4 mm in width, and 20 mm in gauge length. The samples were mounted onto the machine grip and stretched with a strain rate of 0.011s^{-1} until breakage as shown in Figure 1.



Figure 1 Tensile test was conducted using a universal testing machine.

3. RESULTS AND DISCUSSION

The calculated average fibre diameter was 325 ± 51 nm. The produced PVOH nanofibers were smooth and uniform as evidenced by SEM micrograph in Figure 2.

The average tensile strength of PVOH electrospun fibres was 2.5838 MPa as shown in Table 1. The result is compared with previous study; Ismail and Zaaba [6] reported that the tensile strength of PVOH film was about 10.0 MPa. The difference in tensile value as compared to present study was mainly due to different sample structure and test conditions. The most notable difference was the thickness of the nanofibers which in this study was 0.01 mm while in the mentioned study was 0.10 mm.

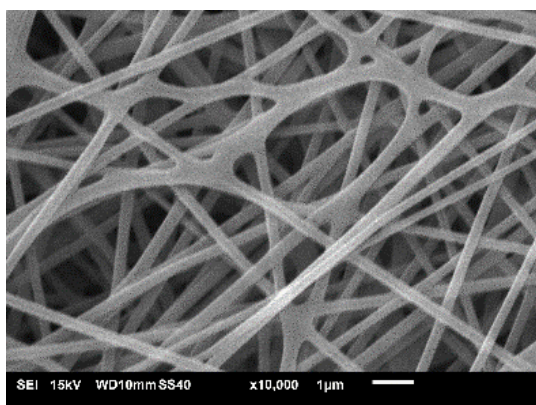


Figure 2 SEM micrograph of electrospun PVOH nanofibers at $\times 10,000$ magnification.

Table 1 Tensile strength of poly (vinyl alcohol) electrospun fibers.

Sample	Tensile strength (TS) (MPa)
1	2.6227
2	2.5654
3	2.539
4	2.3561
5	2.8361
Average	2.5838

4. CONCLUSION

Nanofibres of poly(vinyl alcohol) were successfully produced using electrospinning. From SEM micrograph, smooth and uniform fibres were produced. The average tensile strength of the PVOH electrospun fibers was 2.58 MPa.

ACKNOWLEDGEMENT

This work is funded by FRGS/1/2015/TK10/FKM/02/F00275 Ministry of Education Malaysia. Special thanks to Fakulti Kejuruteraan Mekanikal, Universiti Teknikal Malaysia Melaka (UTeM).

REFERENCES

- [1] Zhou, F. L., & Gong, R. H. (2008). Manufacturing technologies of polymeric nanofibres and nanofibre yarns. *Polymer International*, 57(6), 837-845.
- [2] Lim, C. T. (2017). Nanofiber technology: current status and emerging developments. *Progress in Polymer Science*, 70, 1-17.
- [3] Mirjalili, M., & Zohoori, S. (2016). Review for application of electrospinning and electrospun nanofibers technology in textile industry. *Journal of Nanostructure in Chemistry*, 6(3), 207-213.
- [4] Long, F. C., Nurfaizy, A. H., & Daud, M. A. M. (2016). A preliminary study of greyscale intensity and deposited electrospun fibres using image analysis technique. *Proceedings of Mechanical Engineering Research Day 2016*, 2016, 165-166.
- [5] Lasprilla-Botero, J., Alvarez-Lainez, M., & Lagaron, J. M. (2018). The influence of electrospinning parameters and solvent selection on the morphology and diameter of polyimide nanofibers. *Materials Today Communications*, 14, 1-9.
- [6] Ismail, H., & Zaaba, N. F. (2011, September). Effect of polyvinyl alcohol on tensile properties and morphology of sago starch plastic films. In *2011 National Postgraduate Conference* (pp. 1-3). IEEE.

An investigation on degree of crystallinity of poly(vinyl alcohol) electrospun nanofibers

Abdul Hamid Nurfaizy^{1,2,*}, Nur Hidayah Hashim¹, Zaleha Mustafa³, Mohd Afzanizam Rosli^{1,2}, Muhd Ridzuan Mansor^{1,2}, Nadlene Razali^{1,2}

¹Fakulti Kejuruteraan Mekanikal, Universiti Teknikal Malaysia Melaka, Hang Tuah Jaya, 76100 Durian Tunggal, Melaka, Malaysia

²Centre for Advanced Research on Energy, Universiti Teknikal Malaysia Melaka, Hang Tuah Jaya, 76100 Durian Tunggal, Melaka, Malaysia

³Fakulti Kejuruteraan Pembuatan, Universiti Teknikal Malaysia Melaka, Hang Tuah Jaya, 76100 Durian Tunggal, Melaka, Malaysia

*Corresponding e-mail: nurfaizy@utem.edu.my

Keywords: Electrospinning, electrospun nanofibres, crystallinity, poly(vinyl alcohol)

ABSTRACT – This study investigates the degree of crystallinity of poly(vinyl alcohol) (PVOH) electrospun nanofibres. PVOH fibres were produced using electrospinning process. Differential scanning calorimetry (DSC) was used to examine the degree of crystallinity. The characterization of PVOH electrospun nanofibres was analyzed using scanning electron microscope and Image J software. From the results, electrospun PVOH nanofibres was found to have higher degree of crystallinity compared to raw PVOH. The increase of degree of crystallinity of the polymer was mainly due to mechanical stretching of polymer chains during electrospinning process.

1. INTRODUCTION

Poly(vinyl alcohol) or PVOH has earned a great amount of attention for various applications due to its unique characteristics. PVOH is known to have good mechanical properties, biodegradable and could provide excellent gas barrier. Recently, PVOH has been successfully transformed into nanoscale fibres using a process known as electrospinning. One of the important parameters in the electrospinning is the distance between the tip of the spinneret and the grounded collector [2]. This parameter plays important role in order to produce perfect nanofibres with no defects during electrospinning process occurred.

A typical electrospinning machine has three main components i.e. high voltage power supply, a capillary tube with a small diameter orifice and at grounded collector [1]. According to Huang et. al. [1], due to repulsive electrostatic forces, the applied high voltage will stretch the polymer before being collected at the collector electrode. This mechanical stretching could change the alignment of the polymer molecules, thus affecting the degree of crystallinity of the polymer. However, little is known about the effect of electrospinning process on degree of crystallinity. This study aimed at investigating the effect of electrospinning process on the degree of crystallinity of electrospun fibres.

2. METHODOLOGY

PVOH with molecular weight of 124,000-130,000 g/mol was purchased from Polyscientific, Malaysia.

Samples of PVOH fibres were produced using electrospinning process with time, distance and voltage at 40 minutes, 10cm and 15kV, respectively. The aqueous PVOH solution was prepared at 8 wt.% using mechanical stirrer (IKA RW20, IKA Works, Malaysia) for 6 hours.

The samples were cut to a dimension of approximately 1cm × 1cm. The sample was coated with platinum using an auto fine coater (JEOL JEC-300FL) for 180 seconds and scanned using a scanning electron microscope Model JSM-6010PLUS/ LV (JEOL Ltd., Japan). ImageJ software was used to determine the average diameter of the fibres. Differential scanning calorimetry samples were prepared by peeling the nanofibre mat to a mass of approximately 5 mg. The temperature range was set between 30° to 250°C with the heating/cooling rate set at 10°C/min. The nitrogen flow rate was set at 20 ml/min.

From the enthalpy under the curves, the degree of crystallinity can be calculated by using the following equation:

$$\% \chi_c = \frac{\Delta H_m - \Delta H_c}{\Delta H_m(100\%)} \times 100\% \quad (1)$$

Where ΔH_m is the melting enthalpy, ΔH_c is the crystallization and $\Delta H_m(100\%)$ is the melting enthalpy in J/g of totally crystallized PVOH. In this case for PVOH, the value 138.6 J/g is the melting enthalpy of totally crystallized PVOH.

3. RESULTS AND DISCUSSION

From SEM micrograph, the average fibre diameter of the fibres was 287 ± 25 nm. The thermal properties of nanofibres PVOH and raw PVOH are shown in Table 1. The glass transition temperatures of electrospun fibres taken at 71.8°C and raw PVOH at 71.91°C were observed similar. The enthalpy of melting raw and electrospun fibres, ΔH_m increases from 22.9931 J/g to 28.6842 J/g. The results obtained were comparable to Ricciardi *et al.* [5] who claimed that the increase of ΔH_m was due to increase of degree of crystallinity. Figure 1 and 2 show the DSC cycles of both electrospun fibres and raw PVOH. There were two cycles shown in each of the graph representing heating and cooling rate. The first heating cycle was carried out to eliminate thermal history and moisture content [3]. When the test was carried out on electrospun fibres, it produced larger and broader

endothermic curve since the PVOH nanofibres are highly interacted with water. Meanwhile, raw PVOH sample only show slight endothermic curve at melting temperature (T_m). Overall, the degree of crystallinity

electrospun nanofibres PVOH at 22.14% was higher than raw PVOH at 19.41%. According to Reneker and Yarin [4], the degree of crystallinity increases due to molecular chains stretching during electrospinning.

Table 1 Thermal properties DSC.

Samples	No of cycle (Heating/Cooling rate)	Glass transition	Heat capacity	Melting		Crystallization		% χ_c fibre
		$T_g(^{\circ}\text{C})$	ΔC_p (J/g)	T_m ($^{\circ}\text{C}$)	ΔH_m (J/g)	T_c ($^{\circ}\text{C}$)	ΔH_c (J/g)	
Raw PVOH	1	-	-	189.44	22.9931	107.64	-3.9126	19.41
Fibre PVOH	2	71.91	0.504	-	-	102.78	-1.1527	-
Fibre PVOH	1	55.3	64.7383	190.3	28.6842	93.62	-2.0024	22.14
PVOH	2	71.81	0.539	-	-	90.78	-0.8612	-

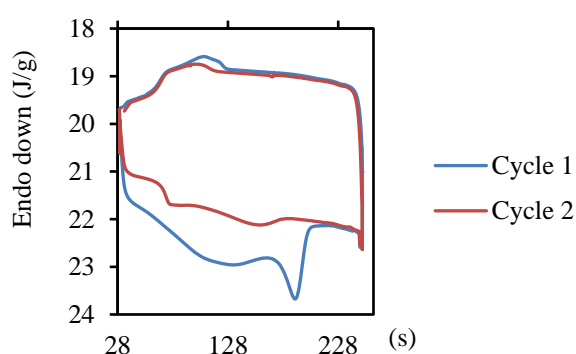


Figure 1 Thermograph of raw PVOH.

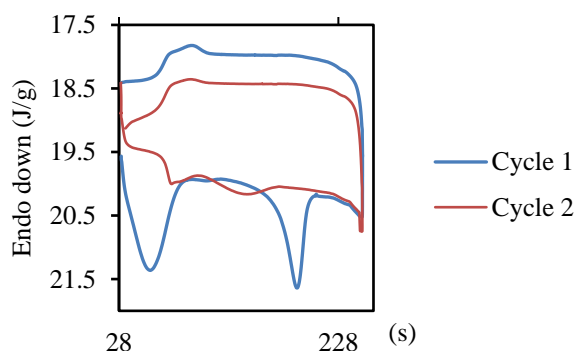


Figure 2 Thermograph of nanofibres PVOH.

4. CONCLUSION

Electrospun PVOH nanofibres from electrospinning process was found to have higher degree of crystallinity compared to raw PVOH. The degree of crystallinity PVOH electrospun fibres was 22.14% which was slightly higher than that of raw PVOH at 19.41%. The increase of degree of crystallinity was due to mechanical stretching of the fibres during electrospinning process.

ACKNOWLEDGEMENT

This work is funded by ANCHOR/2019/FKM-CARE/A00020. Special thanks to Fakulti Kejuruteraan Mekanikal, UTeM.

REFERENCES

- [1] Huang, Z. M., Zhang, Y. Z., Kotaki, M., & Ramakrishna, S. (2003). A review on polymer nanofibers by electrospinning and their applications in nanocomposites. *Composites science and technology*, 63(15), 2223-2253.
- [2] Long, F., Kamsom, R., Nurfaizey, A., Isa, M., & Masripan, N. (2017). The influence of electrospinning distances on fibre diameter of poly (vinyl alcohol) electrospun nanofibres. *Proceedings of Mechanical Engineering Research Day*, 377-378.
- [3] Othman, N., Azahari, N. A., & Ismail, H. (2011). Thermal properties of polyvinyl alcohol (PVOH)/corn starch blend film. *Malaysian Polymer Journal*, 6(6), 147-154.
- [4] Reneker, D. H., & Yarin, A. L. (2008). Electrospinning jets and polymer nanofibers. *Polymer*, 49(10), 2387-2425.
- [5] Ricciardi, R., Auriemma, F., Gaillet, C., De Rosa, C., & Lauprêtre, F. (2004). Investigation of the crystallinity of freeze/thaw poly (vinyl alcohol) hydrogels by different techniques. *Macromolecules*, 37(25), 9510-9516.

Study on modulus of ABS single strut and reclaimed carbon fibre

Rafidah Hasan^{1,2,*}, Zurina Shamsudin³, Muhammad Fakhrur Iqbal Muslim¹, Azira Mat Yusof¹

¹⁾Fakulti Kejuruteraan Mekanikal, Universiti Teknikal Malaysia Melaka, Hang Tuah Jaya, 76100 Durian Tunggal, Melaka, Malaysia

²⁾Centre for Advanced Research on Energy, Universiti Teknikal Malaysia Melaka, Hang Tuah Jaya, 76100 Durian Tunggal, Melaka, Malaysia

³⁾Fakulti Kejuruteraan Pembuatan, Universiti Teknikal Malaysia Melaka, Hang Tuah Jaya, 76100 Durian Tunggal, Melaka, Malaysia

*Corresponding e-mail: rafidahhasan@utem.edu.my

Keywords: Lattice structure strut; reclaimed carbon fibre; tensile test

ABSTRACT – This study focusses in the determination of elastic property for 3D printed ABS single strut specimen and comparison with that of reclaimed carbon fibre (rCF). The study was applied for straight struts using compliance correction method with different gauge lengths of between 8 mm to 30 mm and single fibre testing of the reclaimed carbon fibre at fix gauge length. The tensile test was performed with reference to ASTM D638 standard procedure by using Shimadzu EZ Test (EZ-LX) machine. It was found that a reliable modulus was determined for ABS single strut using compliance correction method, meanwhile, the rCF modulus was strongly correlated with the condition of the tested fibres.


1. INTRODUCTION

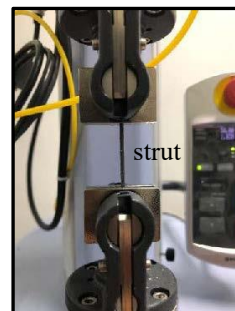
The applications of lattice structures are widely used in additive manufacturing (AM) in recent years. Now, studies proved that open-pored cellular lattice structures with more complex geometrical structures are able to be created where the structures are mostly in regular rectangular forms and mostly used in heat exchangers or filter elements [1]. Lattice structure is a lightweight material with the properties of high stiffness and strength-to-weight scaling where the assembly methods of the strut-based lattice structure require a flexible configuration for complex geometrical designs as well as its mechanical properties [2,3]. Lattice structure comprises of many struts connected to each other by nodes, in many architectural arrangements such as body-centred-cubic (BCC), face-centred-cubic (FCC) and hexagonal close -packed (HCP) where possible architectural arrangements can be proposed [4]. The value for mechanical properties, the performance and the quality of lattice structure can be concluded through an examination of struts thus making struts as a fundamental element for lattice structure [5]. Meanwhile, reclaimed carbon fibre (rCF) has been explored and its potential as reinforcement in composite is still under study, especially to enhance the properties of modulus. Therefore, this research is examining the single strut under tensile loading, which lead to the determination of elastic modulus for 3D printed ABS strut and comparison with that of values of the rCF, in order to provide useful information for selection of excellent structure to benefit industrial applications.

2. METHODOLOGY

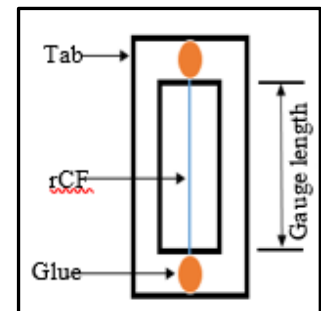
ABS single strut was designed by using CATIA with 1.6 mm diameter, at 35.26° build angle, in order to represent the strut position in BCC lattice structure material. The designed single strut was then fabricated by using CubePro 3D printer machine, using 200 µm layer resolution, ‘Solid’ print strength, and ‘Cross’ print pattern. Strut specimens with five different lengths were produced as shown in Table 1. Tensile test was done on the specimens as shown in Figure 1(a), using 1 kN load cell at rate 0.1 mm per minute. Compliance correction method [5] was applied in the analysis of elastic modulus value. Meanwhile, the rCF was received in pyrolised form with diameter between 7 µm to 8 µm and 10 fibres were mounted on rectangular frame at fix gauge length of 25 mm as illustrated in Figure 1(b). The load cell was also rated to 1 kN with similar constant rate displacement.

Table 1 Specimens with different lengths for ABS strut.

Specimen Length, mm	Gauge Length, mm	Appearance
24	8	
45	15	
50	20	
75	25	
90	30	



(a)



(b)

Figure 1 Tensile test arrangement for (a) ABS single strut and (b) rCF specimen (schematic).

3. RESULTS AND DISCUSSION

The modulus of elasticity for ABS single strut was determined by calculating the gradient of the best-fit line on each stress-strain graph for each gauge length. Each gauge length produced different value of elastic modulus, hence, further analysis using compliance correction method [5] was carried out to determine a reliable and robust value of elastic modulus for the single strut.

Apparent compliance, C_a was obtained from force against elongation of specimen. Plot of apparent compliance, C_a against length L over square of diameter D^2 , has produced the value of machine compliance, C_m . This is shown in Figure 2.

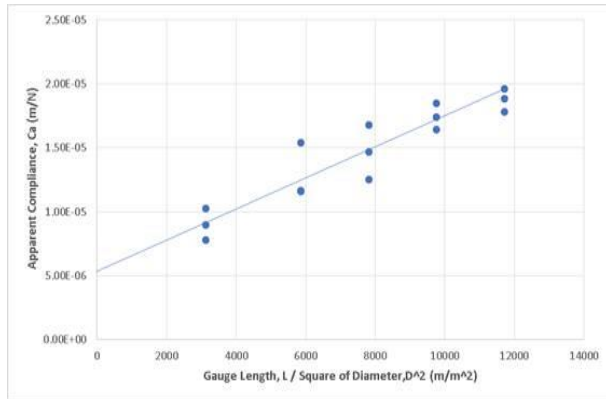


Figure 2 Plot of C_a against L/D^2 .

Equation (1) was used to determine elastic modulus values, E for all gauge lengths. E_u is uncorrected elastic modulus, determined directly from stress-strain graph for each gauge length. Table 2 shows the results of corrected elastic modulus values for ABS 3D printed single struts.

$$E = \frac{E_u \cdot C_a}{C_a - C_m} \quad (1)$$

Table 2 Corrected elastic modulus value for ABS strut.

Gauge Length, mm	Apparent Compliance, C_a	Un-corrected Elastic Modulus, E_u (MPa)	Corrected Elastic Modulus, E (MPa)
8	9.03×10^{-6}	315.6 ± 56	1095.1 ± 139
15	12.9×10^{-6}	545.5 ± 57	1036.6 ± 227
20	14.7×10^{-6}	625.3 ± 44	1067.8 ± 179
25	17.3×10^{-6}	684.2 ± 36	1040.6 ± 87
30	18.8×10^{-6}	749.3 ± 48	1199.3 ± 95
Average corrected value			1087.9 ± 146

It can be observed that the corrected values are all similar, with average value of 1087.89 ± 145 MPa. Thus, this has eliminated the uncertain various values of elastic modulus from different gauge lengths. The determined elastic modulus value is found as comparable to that of standard value of ABS elastic modulus (between 1100 to 2900 MPa). However, for rCFs modulus were calculated directly and average modulus was between 120 to 170 MPa. A low value indicates there is a wide range of flaw size in the fibres as shown in Figure 3.

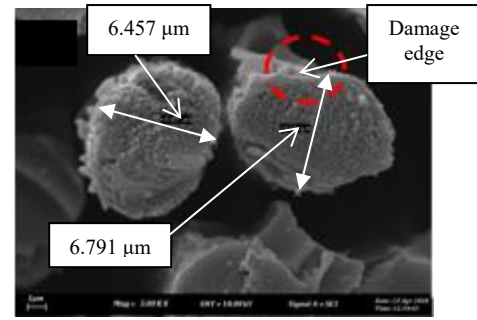


Figure 3 Flaw at edge of the rCF.

4. SUMMARY

Strut is a basic unit of lattice structure material, and it is an important part to be characterized. The result from this study shows that a reliable and robust elastic modulus value of single strut can be determined by using compliance correction method, thus eliminate the uncertain values that are affected by different gauge lengths. The corrected elastic modulus value is found as comparable to that of standard property, thus can be used in future analysis of lattice structure material. The rCF modulus shows variation in values and the low values are likely to be caused by the introduction of further surface flaws during processing and handling.

ACKNOWLEDGEMENT

Authors gratefully acknowledge Universiti Teknikal Malaysia Melaka (UTeM) for facilities and financial supports. This research was partially supported by short-term grant PJP/2018/FKP(9A)/S01590.

REFERENCES

- [1] Afshar, M., Anaraki, A. P., Montazerian, H., & Kадkhodapour, J. (2016). Additive manufacturing and mechanical characterization of graded porosity scaffolds designed based on triply periodic minimal surface architectures. *Journal of the mechanical behavior of biomedical materials*, 62, 481-494.
- [2] Al-Ketan, O., Rowshan, R., & Al-Rub, R. K. A. (2018). Topology-mechanical property relationship of 3D printed strut, skeletal, and sheet based periodic metallic cellular materials. *Additive Manufacturing*, 19, 167-183.
- [3] Hasan, R., Mines, R. A., Shen, E., Tsopanos, S., & Cantwell, W. (2011). Comparison on compressive behaviour of aluminium honeycomb and titanium alloy micro lattice blocks. In *Key Engineering Materials*, 462, 213-218.
- [4] Azman, A. H. (2017). *Method for integration of lattice structures in design for additive manufacturing* (Doctoral dissertation, Université Grenoble Alpes).
- [5] Hasan, R., Mines, R. A. W., & Tsopanos, S. (2010). Determination of Elastic Modulus Value for Selectively Laser Melted Titanium Alloy Micro-Strut. *Journal of Mechanical Engineering and Technology*, 2(2), 17-25.

Design of bamboo bending tools on bird cage making based on anthropometric analysis

Teguh Aprianto*, Herman Ruswan Suwarman, Mochamad Saidiman

Sekolah Tinggi Teknologi Bandung, Soekarno-Hatta St No.378, Kebon Lega, Bojongloa Kidul, Bandung City, West Java 40235, Indonesia

*Corresponding e-mail: teguh@sttbandung.ac.id

Keywords: Bamboo bending tools; bird cage making; anthropometric analysis

ABSTRACT – The high number of bird enthusiasts has increased the need for bird cages. The frame material for making bird cages is usually made of bamboo, wood, rattan, metal and plastic. The Government of Garut Regency, West Java, developed the North Garut area in Selaawi District as a bamboo handicraft tourism to grow the economy of the people who mostly work as bamboo craftsmen. Bird cage business is able to bring profits that can be said big. Cage making still uses simple equipment and takes a long time in making it. One of the processes in the manufacture of cages is the bending of bamboo bird cages in Selaawi sub-district still using human power by heating bamboo then bending using the legs. For this reason, it is necessary to make improvements in the bending process, namely by designing a bamboo bent in the manufacture of bird cages in Garut regency. So that the results of bird cages increase and can meet consumer needs. The design is based on anthropometric analysis, thus, in this study samples were taken from workers to obtain the desired dimensions.

1. INTRODUCTION

The use of bamboo plants in Indonesia has been going on for a very long time. Our rural communities have used bamboo since ancient times for various life support purposes, such as making houses or household furniture. As a herbaceous plant, bamboo also has strong and flexible stems. Bamboo plants are also used as material for making bird cage frames.

The birds singing with their sweet voice makes birds chirp with many fans. The high number of bird enthusiasts has increased the need for bird cages. The frame material for making bird cages is usually made of bamboo, wood, rattan, metal and plastic. The Government of Garut Regency, West Java, developed the North Garut area in Selaawi District as a bamboo handicraft tourism to grow the economy of the people who mostly work as bamboo craftsmen.

Residents in Selaawi Subdistrict have 39 thousand inhabitants, around 1,900 of them work as bamboo artisans making bird cages, home appliances and various other interesting accessories. The opportunity for a bird cage business is one of the most profitable businesses. Bird cage business is able to bring profits that can be said big. The bird cage business is indeed not a new business, but the opportunity is very large. The prospect of a bird cage business can indeed be said to be very promising. Day after day the demand for bird cages continues to increase. In running a bird cage

business requires raw materials for its manufacture. To make bird cages requires raw materials, namely bamboo.

In the process of making cages, craftsmen still use simple and manual equipment. Cage making still uses simple equipment and takes a long time in making it. One of the processes in the manufacture of cages is the bending of bamboo bird cages in Selaawi sub-district still using human power by heating bamboo then bending using the legs.



Figure 1 The process of making bird cages.

For this reason, it is necessary to make improvements in the bending process, namely by designing a bamboo bent in the manufacture of bird cages in Garut regency. So that the results of bird cages increase and can meet consumer needs.

2. METHODOLOGY

The research method uses anthropometric analysis to design the bending tools. Bird cage craftsmen were taken as research sample to meet the desired ergonomic dimension. The research was done by steps illustrated in Figure 2.

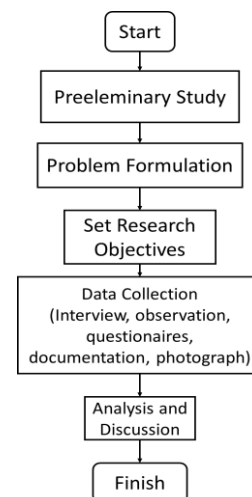


Figure 2 Research flow chart.

3. RESULTS AND DISCUSSION

Anthropometric data used are body dimensions needed in the design of bamboo bending in the manufacture of bird cages in Selaawi district, Garut Regency. The collection process was carried out to obtain the dimension needed in the design of bamboo bending in the manufacture of bird cages in Selaawi sub-district, Garut Regency. In designing bamboo bending (Figure 3) in the manufacture of bird cages in Selaawi District, Garut Regency, anthropometric data is needed. The steps of data processing are explained below:

Step 1 The data is processed before the design is carried out, namely the distribution of questionnaires, drafting of draft concepts, processing of anthropometric data and design of bamboo bending in the manufacture of bird cages in Selaawi sub-district, Garut Regency.

Step 2 Body dimension data was tested using data normality test, uniformity test and data adequacy test.

Step 3 Percentile calculation

Percentile values can be determined from the table of normal distribution probabilities. Percentile is a range that can be used. 5th percentile, the calculation is: $X - 1.645 \cdot SD$; 50th percentile, calculation is: X ; 95th percentile, the calculation is: $X + 1.645 \cdot SD$

Step 4 Design of bamboo bending in the manufacture of bird cages

In this process what will be made is a bamboo bending tool for making bird cages in Selaawi sub-district, Garut Regency

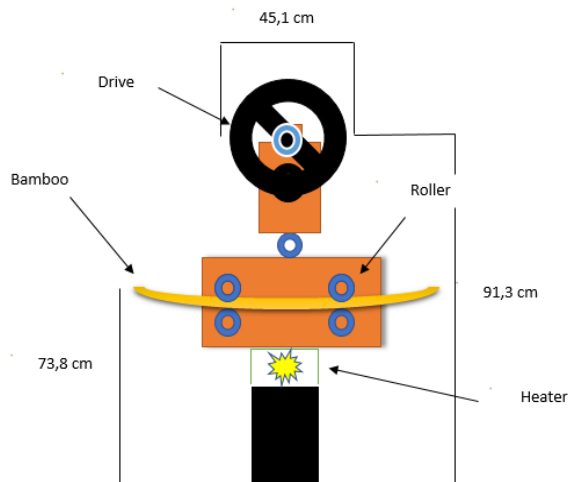


Figure 3 Bamboo bending design on bird cage making.

4. CONCLUSIONS

- Design of bamboo bending in the manufacture of bird cages has height 91,3 cm, drive 45,1 cm, height of bamboo on the roller is 73,8 cm
- Using anthropometric data is shoulder width, elbow height of standing position, knuckle height of standing position
- Design of bamboo bending in the manufacture of bird cages has dimension ergonomic

REFERENCES

- Anonim. (2019). Bambu sebagai tanaman konservasi. Received online: <http://www.medcofoundation.org/bambu-sebagai-tanaman-konservasi/>
- Feri. (2017). Garut utara dikembangkan sebagai wisata kerajinan bambu. Received online: <https://jabar.antaranews.com/berita/62378/garut-utara-dikembangkan-sebagai-wisata-kerajinan-bambu>.
- Kurniawan, A. (2012). Asal usul tanaman bambu. Received online: <http://www.neraca.co.id/article/8948/asal-usul-tanaman-bambu>
- Nurmianto, E. (2008). Ergonomi konsep dasar dan aplikasinya, GunaWidya.
- Suwandi, D. (2015). Mengenal tanaman bambu. Received online: <https://dapurawi31.wixsite.com/bambu-indonesia/single-post/2015/02/22/Mengenal-Tanaman-Bambu>
- Tarwaka, S., & Lilik. (2004). Ergonomi untuk keselamatan, kesehatan kerja dan produktivitas, Uniba Press, Surakarta.
- Tarwaka. (2014). Ergonomi industri: Dasar-dasar pengetahuan ergonomi dan aplikasi di tempat kerja. Harapan Press Surakarta.
- Wiginosoebroto, S. (1995). Ergonomi studi gerak dan waktu, Guna Widya.

Prediction of crack propagation direction in fretting fatigue

M.H. Maslan*, O. Ifayefunmi, M.A.A. Wahap

Fakulti Kejuruteraan Mekanikal, Universiti Teknikal Malaysia Melaka,
Hang Tuah Jaya, 76100 Durian Tunggal, Melaka, Malaysia

*Corresponding e-mail: haidir@utem.edu.my

Keywords: Fretting fatigue; finite element; crack propagation

ABSTRACT – Nucleation and propagation of cracks under fretting conditions has been a subject of study for many years. The aim of this research is to predict crack propagation direction in complete contact fretting fatigue. This study uses the earlier experimental results with Royal Aerospace Establishment (RAE Farnborough) as the reference for comparison. Two crack propagation criterions, Maximum Tangential Stress (MTS) and Maximum Tangential Stress Range (Δ MTS) are compared using a commercial finite element code, ABAQUS. Results clearly show that Maximum Tangential Stress Range (Δ MTS) can become good estimation tool for predicting crack propagation direction in complete contact fretting fatigue.

1. INTRODUCTION

Correct crack path is important on modelling in analysing crack propagation especially for small crack. Difference crack angle influenced value of stress intensity [1] and affecting crack propagation analysis as crack length is now has been differ as the crack is kinked out. Hence, the determination of accurate crack path become significant in order to make better prediction of specimen life under cyclic loading.

In this study, two criterions that have been proved to work well for complete contact crack direction is compared. Those criterions are Maximum Tangential Stress (MTS) based on study by Faanes [2] and Maximum Tangential Stress Range (Δ MTS) based on study by Giner [3]. Faanes do the analysis using mathematical equation to determine stress intensity factor in mode I and mode II. These values is then determine using stress in front of crack tip. Meanwhile, Giner analysed with the aid of ABAQUS on a single pad complete contact.

2. MODEL DESCRIPTION

The basis for this study is the Royal Aerospace Establishment (RAE Farnborough) experimental works of Sheikh et al [1]. In his work, a general fretting fatigue test apparatus was used which consisted of flat fretting bridge pads over a specimen of rectangular cross section.

The material investigated was BS-L65, a fully artificially aged 4 percent copper aluminium alloy (also known as Al 2014). The fretting pads were made of BS S98 steel (2.5% Nickel-Chrome-Moly steel. Table 1 gives the elastic properties of these materials.

Table 1 Materials properties.

Materials	Young Modulus, E	Poisson Ratio, ν	Yield Stress, σ_y
BS L65	74.0 GPa	0.33	420 MPa
BS S98	210 GPa	0.29	1002 MPa

Due to symmetry, a quarter 2D finite element model has been used to represent the fretting fatigue tests, as shown in Figure 1. Since the specimen is 8 mm thick, plane strain elements are used in the analysis. Mesh is refined towards the edges of contact region with a coarse mesh away from the contact region to reduce processing time. Matched meshes are used on the master and slave contact surfaces.

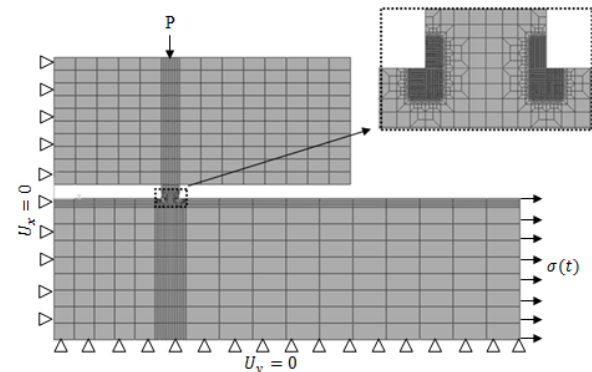


Figure 1 Finite element model of a quarter of the fretting specimen-pad arrangement.

A Lagrange multiplier contact algorithm is used to strictly enforce the sticking condition when shear stress is less than the critical value according to the Coulomb friction law [4].

The loading history is represented in Figure 2. In the first analysis step, a normal load, P is applied to the fretting pads. In the next step, the specimen is loaded by a cyclic fatigue load $\sigma(t)$ with a maximum value σ_{max} and a stress ratio of $R = -1$.

In ABAQUS, crack is modelled using embedded line, which known as “seam” in ABAQUS. In order to get better results, mesh refining toward the crack tip is required. Partitioning strategy is used to create the desired crack and to facilitate the generation of uniform focused mesh.

In order to obtain the maximum value of MTS or Δ MTS, K_I and K_{II} values obtained from each simulation are used to calculate the tangential stress ($\sigma_{\theta\theta}$). θ is varied for each degree and plotted to get the maximum tangential stress angle and maximum tangential stress range.

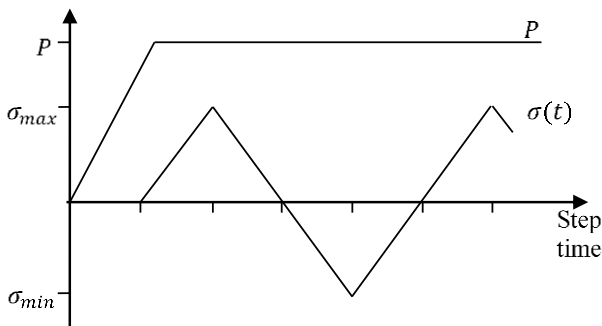


Figure 2 Normal load and cyclic axial load history applied to the finite element model.

3. RESULTS AND DISCUSSION

Figure 3 shows the results from the analysis. In overall, Δ MTS give better prediction compared to MTS criterion.

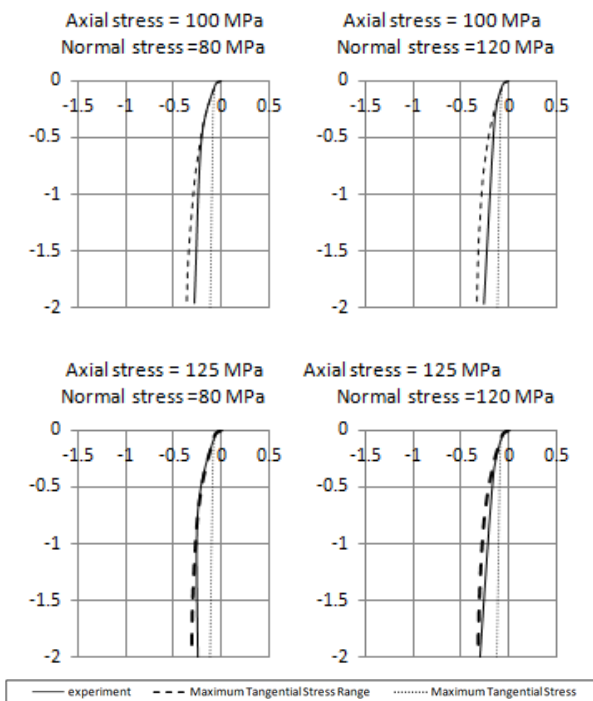


Figure 3 One-column illustration.

Although Both criterions assumed that crack will propagate to the direction where tangential stress is maximum, MTS only consider stress field in front of crack tip at particular time when the tangential stress is maximum only which will occur when the axial stress applied is in tension. While Δ MTS consider stress field in a range of time for one complete cycle.

Contact Stress during maximum tension and compression axial stress can be observed in Figure 4. It can be seen that there is no contact stress occur at the

surface near leading edge in tension loading. But the contact stress is very high in maximum compressive cycle due to slightly small rotation movement by the fretting pad. In other word, in maximum tensile loading, the stress in front leading edge is almost like specimen with only uniaxial stress without the contact effect. This may be the reason why MTS crack is almost a straight. Meanwhile, Δ MTS that consider stress field for a cycle able to use the multi axial effect in the prediction.

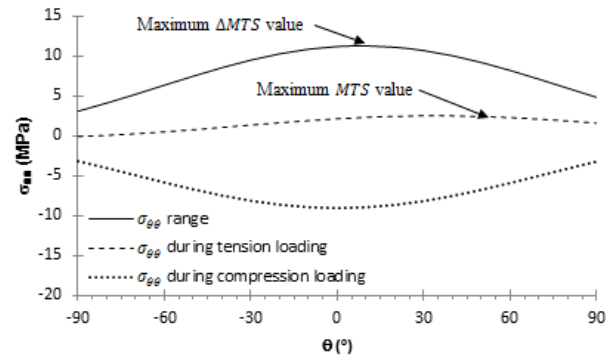


Figure 4 Example of $\sigma_{\theta\theta}$ value over 180° range.

4. CONCLUSION

From the results, it can be concluded that Δ MTS criterion can provide a good estimation tool for estimating crack propagation direction in complete contact fretting fatigue.

ACKNOWLEDGEMENTS

The authors would like to acknowledge the financial support received from University Teknikal Malaysia Melaka (UTeM) and the Ministry of Education Malaysia under Fundamental Research Grant Scheme FRGS/2018/FTKMP-CARE/F00386

REFERENCES

- [1] Sheikh, M. A. (1994). Elastic stress intensity factors for fretting cracks using the finite element method. *Fretting Fatigue*, 83.
- [2] Faanes, S. (1995). Inclined cracks in fretting fatigue. *Engineering Fracture Mechanics*, 52(1), 71-82.
- [3] Giner, E., Sabsabi, M., Ródenas, J. J., & Fuenmayor, F. J. (2014). Direction of crack propagation in a complete contact fretting-fatigue problem. *International Journal of Fatigue*, 58, 172-180.
- [4] ABAQUS, *ABAQUS 6.11 Analysis User's Manual*. Dassault Systèmes, Providence, RI, USA, 2011.